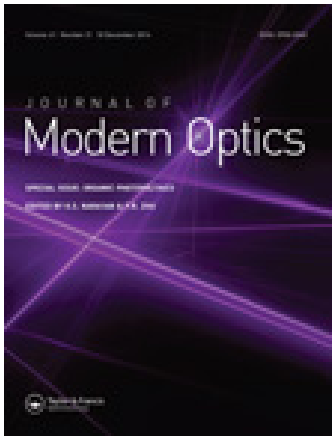

Journal of Modern Optics
Publication details, including instructions for authors and subscription information:
http://www.tandfonline.com/loi/tmop20

Organic semiconductor-based photonic crystals for solar cell arrays: band gap and optical properties

Filiz Karaomerlioglu[ab], Amirullah M. Mamedov[bc] & Ekmel Ozbay[b]
[a] Department of Electrical and Electronics Engineering, Mersin University, Mersin, Turkey
[b] Nanotechnology Research Center, Bilkent University, Ankara, Turkey
[c] International Scientific Center, Baku State University, Baku, Azerbaijan
Published online: 10 Oct 2014.

To cite this article: Filiz Karaomerlioglu, Amirullah M. Mamedov & Ekmel Ozbay (2014) Organic semiconductor-based photonic crystals for solar cell arrays: band gap and optical properties, Journal of Modern Optics, 61:21, 1754-1760, DOI: 10.1080/09500340.2014.967320

To link to this article: http://dx.doi.org/10.1080/09500340.2014.967320

Journal of Modern Optics, 2014
Vol. 61, No. 21, 1754–1760, http://dx.doi.org/10.1080/09500340.2014.967320

Organic semiconductor-based photonic crystals for solar cell arrays: band gap and optical properties

Filiz Karaomerlioglu[a,b]*, Amirullah M. Mamedov[b,c] and Ekmel Ozbay[b]

[a]*Department of Electrical and Electronics Engineering, Mersin University, Mersin, Turkey;* [b]*Nanotechnology Research Center, Bilkent University, Ankara, Turkey;* [c]*International Scientific Center, Baku State University, Baku, Azerbaijan*

(*Received 24 March 2014; accepted 12 September 2014*)

Photonic crystals (PCs) hold great potential for designing new optical devices because of the possibility of the manipulation of light with PCs. There has been an increase in research on tuning the optical properties of PCs to design devices. We design organic semiconductor-based PC structures and calculate optical properties using the plane wave expansion method and finite-difference time-domain method in an air background for a hexagonal lattice. We showed the possibility of the solar cell arrays for a 2D PC cavity on an organic semiconductor base infiltrated with a nematic liquid crystal. E7 type has been used as a nematic liquid crystal and 4,4′-Bis[4-(diphenylamino) styryl]biphenyl as an organic semiconductor material.

Keywords: organic semiconductor; photonic crystal; liquid crystal

1. Introduction

Progress in solid-state physics, optics of 3D artificial structures, and nanotechnologies based on a variety of the physical and chemical processes has strongly stimulated and motivated the investigation into the properties of photonic crystals (PCs) and has resulted in the growth of applications of photonic band gap (PBG) materials [1,2]. The basic feature of PCs is the presence of permitted and forbidden frequency bands for light. It is possible to manipulate the light with PCs. Due to this property, PCs hold great potential for designing new optical devices. Some tunable PBG research has been conducted on one-dimensional (1D), two-dimensional (2D), and three-dimensional (3D) [3–6] PCs.

Providing enough energy to meet the ever-increasing demand is one of the greatest problems the world is now facing. In many countries of the world, much interest is being shown in alternative energy sources. A promising source of energy that would be able to solve a part of the energy crisis for the present and future, by instructively looking at the current technical and economic energy picture as well as sustainable energy is the solar cell (SC). Making a highly efficient SC is always a challenging task for today's scientists and engineers. A lot of research has been carried out on and quite a few approaches have been found to be efficient, such as:

(1) To select semiconductor materials with appropriate energy gaps in order to match the solar spectrum optimizing their optical, electrical, and structural properties; and

(2) Innovative device engineering that enables more effective charge collection as well as better utilization of the solar spectrum through single and multi-junction approaches [5,7].

Increasing the efficiency of SCs by reducing the reflectance on their front surface has been a widely studied issue in recent decades. Traditionally, the performance of SCs can be enhanced significantly by employing PCs. They can either be used as omnidirectional, broadband antireflection coatings (ARCs), or applied to thin-film SCs.

PCs might have a huge impact in this regard. These are artificial materials engineered to have properties that may not be found in nature that would be advantageous for utilizing the whole solar spectrum. In addition, PCs are insensitive to polarization, which can be used to precisely control the path of visible light regardless of the polarization of the light. Responding to these motivations, the authors intended to propose a new innovative approach to integrate PCs as ARC with traditional structures. The design parameters of PC-based SC are conventional semiconductor parameters, emitter and base, grid pattern, ARC, doping, band gap, diffusion length, air mass, etc. Simulation results also support the whole design in terms of efficiencies and usability [8,9].

In view of the achievements in the production of highly efficient light-sensitive devices based on polymeric and organic compounds, these materials are also of considerable interest for the fabrication of PCs [7,10–13].

*Corresponding author. Email: filizkrm@mersin.edu.tr

It is well known that organic semiconductors play an important role in the development of materials for photonics. Organic semiconductors are relatively inexpensive, can be functionalized to achieve the required optical or electronic properties, and have demonstrated their compatibility with various patterning methods. Organic semiconductors can be used as materials for photonic applications in several ways. First, organic semiconductors in themselves can possess useful optical properties. Second, organic semiconductors can act as matrices for optically active species (liquid crystals, dyes, quantum dots, metallic nanoparticles). Finally, organic semiconductors with periodic structures that are useful for photonic applications can be fabricated by nanoimprinting, photolithography, and sequential deposition of alternating organic semiconductor layers [7,11–13].

PCs obtained from organic semiconductors possess an intrinsically low value of Δn originating from the relatively low refractive index of organic semiconductors, and as a result these materials do not possess a full band gap.

In recent years, there has been much interest in the development of artificial electromagnetic structures (PCs). PCs usually gain their properties from the structure rather than the composition, using small inhomogeneities to create effective macroscopic behavior. PCs can be classified according to the response in the presence of an electromagnetic field, broadly on the macroscopic parameters ε and μ of these materials. The thinnest material-based PCs used to fully capture light are limited to a very narrow range of wavelengths and the angles of incidence (for reflectance from the structure). A design composed of a pattern of wedge-shaped ridges whose widths are precisely tuned to slow and capture light of a wide range of wavelengths and the angles of incidence was proposed. These PCs could be made extremely thin, thereby saving weight and cost. In addition, in [17–21], a design of a multilayer sawtooth structure has been proposed in order to absorb a wide range of frequencies with an efficiency of more than 95 percent [22–25].

The light of different wavelengths is absorbed by the material at different levels, where the light's wavelength matches the width of the ridges.

In the case of a general SC, we get only one band gap and only a portion of visible light can be absorbed by SC. However, by using an artificial structure the PC band gap can be tuned.

In the present paper, we investigated BDAVBi-based PC and calculated the energy band structure and optical properties of it (structure was included as the active substrate and PC (ARC) the same material – organic semiconductor and, therefore, we may increase the power conversion of SCs in this structure) by using the plane wave expansion (PWE) and finite-difference time-domain (FDTD) methods.

Figure 1 shows the chemical structure of BDAVBi, which is a hole-conducting material. Because of the linear molecular shape, BDAVBi molecules are significantly oriented in the horizontal direction in vacuum-deposited amorphous films leading to the large optical anisotropy and a much higher refractive index in the horizontal direction (ordinary refractive index, $n_0 = 1.99$) than in the vertical direction (extraordinary refractive index n_e) [14,15].

2. Calculation method

The fundamentals of the PWE and FDTD methods are based on a direct numerical solution of time-dependent Maxwell's equations as shown [16].

On the other hand, Bloch's theorem [17] is used to expand the $H(\vec{r})$ field in terms of plane waves since the light waves are transmitted in periodic structures, as

$$H(\vec{r}) = \sum_{\vec{G}} h\left(\vec{G}\right)\hat{e}_{\vec{G}}e^{i\left(\vec{k}+\vec{G}\right)\cdot\vec{r}} \tag{1}$$

where $\vec{k}$ is a wave vector in the Brillouin zone of the lattice and $\hat{e}_{\vec{G}}$ is the direction that is perpendicular to the wave vector $\left(\vec{k}+\vec{G}\right)$ owing to the transverse character of the magnetic field $H(\vec{r})$, $\nabla \cdot H(\vec{r}) = 0$.

3. Numerical results and discussion

The PC structure that is composed of a PC in organic semiconductor rods infiltrated with nematic LCs in an air background is designed for the hexagonal lattice using the PWE and the FDTD methods. PC structures that are designed as round rods with a hexagonal lattice shape are computed. BDAVBi was used as organic semiconductor material and E7 type as nematic LCs.

This paper is aimed at describing and comparing organic semiconductor-based 2D PC structures that differ by the characteristics of their band gap, transmission, and equi-frequency dependences for SC arrays.

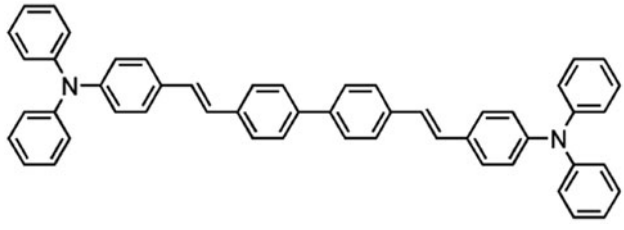

Figure 1. Molecular structures of 4,4′-Bis[4-(diphenylamino) styryl]biphenyl (BDAVBi) used in this study [14].

3.1. Band gap and transmission

We considered the results obtained from the calculation of the band structure of the spectrum for the sample of the 2D PC of the BDAVBi rods type, which consists of the elements in the form of dielectric cylinder forming a hexagonal lattice filled without and with LC. The calculations are performed for the PCs with the ordinary refractive index of the BDAVBi cylinders 1.99 at 532 nm and the period of the structure $a = 1$ μm. E7 type LCs have two different principle refractive indices as the ordinary refractive index $n_0 = 1.5282$ and the extraordinary refractive index $n_e = 1.7558$.

Schematic views of the proposed 2D PC of BDAVBi round rods with nematic LC infilled in an air background ($\varepsilon_a = 1$) in a hexagonal lattice are shown in Figure 2.

The photonic band structure for TE and TM mode is calculated along the direction that includes the high symmetry points, Γ, M, and K for the Brillouin zone in a hexagonal lattice. It is assumed that $r_1 = 0.3a$ denotes the radius of BDAVBi round rods, and $r_2 = 0.15a$ rods LC infilled.

There is no band gap for 2D PC of BDAVBi round rods, rods with air infilled, and rods with nematic LC infilled in TE mode.

Firstly, the 2D PC of BDAVBi round rods is designed for the hexagonal lattice. Figure 3 shows the seed band structure of the PC with the permittivity of the dielectric cylinders. This PC has a maximum width of the first complete band gap. In this case, the PC band gap along the direction between high symmetry points in the $\Gamma - M$ direction of the Brillouin zone lies in the frequency range from $0.380(2\pi c/a)$ to $0.462(2\pi c/a)$ and from $0.693(2\pi c/a)$ to $0.767(2\pi c/a)$.

For BDAVBi round rods, relative widths are 19.43% between band 1 and band 2 and 10.26% between band 3 and band 4 of TM mode.

Supposing the radius of the cylinders, $r_2 = 0.15a$ the photonic band structure of the PC with BDAVBi round rods with air infilled for a hexagonal lattice in an air background are depicted in Figure 4. The band gap has relative

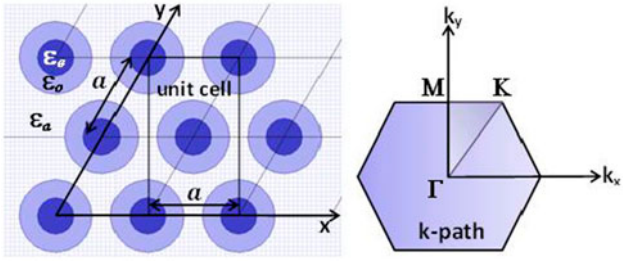

Figure 2. 2D PC structure for a hexagonal lattice BDAVBi round rods in an air background. (The colour version of this figure is included in the online version of the journal.)

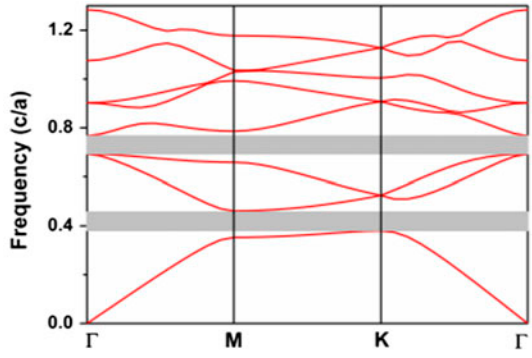

Figure 3. In TM mode, the photonic band structure of BDAVBi round rods with an ordinary refractive index in an air background in a hexagonal lattice. (The colour version of this figure is included in the online version of the journal.)

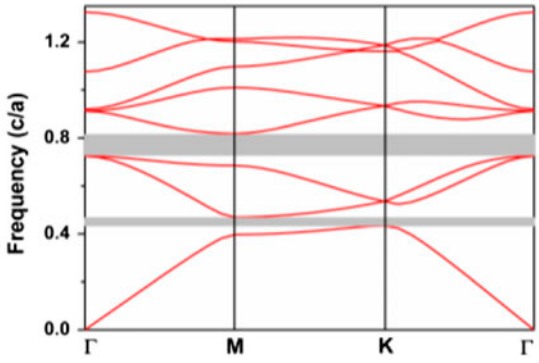

Figure 4. In TM mode, the photonic band structure of BDAVBi round rods with an air infilled in an air background in a hexagonal lattice. (The colour version of this figure is included in the online version of the journal.)

widths of 8.00% between band 1 and band 2 and 12.10% between band 3 and band 4, and center-normalized frequencies of $0.452(2\pi c/a)$ and $0.772(2\pi c/a)$ in TM mode. When 2D PC of BDAVBi round rods with air infilled is compared with BDAVBi round rods in a hexagonal lattice, it is seen that there is a variation in the band gap and frequency values are shifted.

The dispersion of the PC structure in combination with the dispersion of the LC leads to the appearance of changed band gaps in the continuous spectrum of the seed PC and changed transmission bands in the band gap of the PC. These effects are illustrated in Figure 5. It can be seen from Figure 5 that the presented fragment of the band structure of the spectrum exhibits a changed band gap with the width $\Delta\omega = \omega - \omega_0$. This width exceeds the width of the LC resonance lines by an order of magnitude when the frequencies of the LC $0.395(2\pi c/a)$ and $0.464(2\pi c/a)$ are in the continuous spectrum near the low-frequency edge of the first band gap.

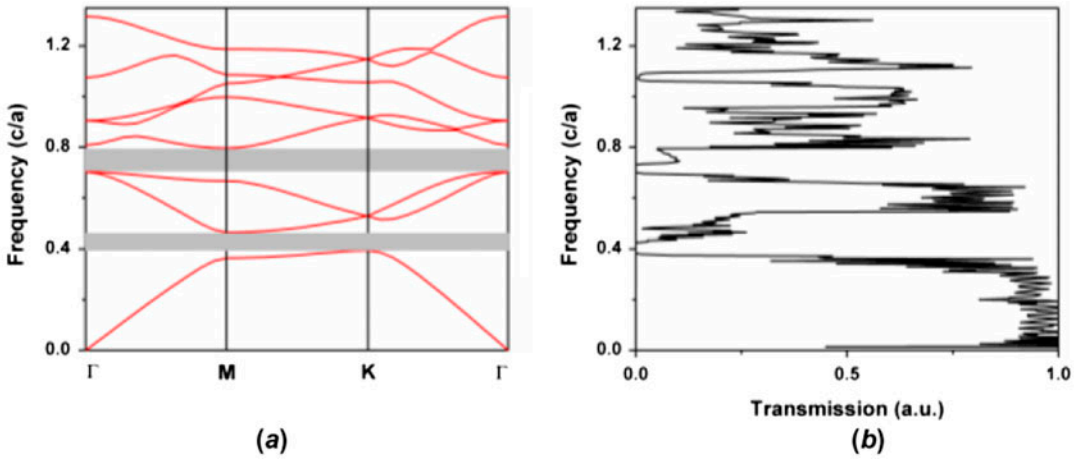

Figure 5. In TM mode (*a*) The photonic band structure (*b*) Transmission spectrum of BDAVBi round rods with nematic LC infilled with an extraordinary refractive index in an air background in a hexagonal lattice. (The colour version of this figure is included in the online version of the journal.)

A different situation arises when the LC frequencies $0.395(2\pi c/a)$ and $0.703(2\pi c/a)$ are in the band gap of the PC (Figure 5). In this case, a changed transmission band with the width exceeding the width of the LC lines by an order of magnitude appears in the band gap.

The widths of the changed transmission band and the band gap can be controlled by varying the type of nematic LC.

When BDAVBi round rods are infiltrated with nematic LC, a two-band gap in TM mode for the extraordinary refractive index is shown in Figure 5(*a*). The band gap has relative widths of 16.19% between bands 1 and 2 and 12.51% between bands 3 and 4, and center-normalized frequencies of $0.430(2\pi c/a)$ and $0.750(2\pi c/a)$. As the results obtained for the ordinary refractive index and extraordinary refractive index of nematic LC are different, it is an indication of anisotropy. Using the anisotropic features of LCs, different results for TE and TM mode were obtained. This means that either the structure is rotated into a certain direction or it is infiltrated with LCs that have different directors (orientations of the LCs molecules along the order's direction) into the structure in order to be able to change the features of these structures.

It is well known that an anisotropic nanostructuring photonic band structure array is capable of changing the polarization state of transmitted or reflected light. Therefore, we also calculated the optical response of the photonic band structure for different directors of the LCs and the light polarization transmitted through a photonic band array. The numerical results of the variation of full transmission by changing the director of LC for the PC structure are presented. The transmission spectrum as a function of the frequency is computed for an extraordinary refractive index of nematic LC in a hexagonal lattice. The transmission of BDAVBi round rods with nematic LC infiltrated is zero at frequencies between $0.384(2\pi c/a)$ and $0.426(2\pi c/a)$, and between $0.700(2\pi c/a)$ and $0.730(2\pi c/a)$ (Figure 5(*b*)).

Let us turn to the analysis of the results obtained from the calculation of the band structure of the spectrum for the sample of a PC infiltrated by LC of the BDAVBi round rods type, which consists of elements in the form of infinite hollow cylinders that are filled with an LC and form hexagonal lattice in a dielectric matrix. Figure 3 shows the seed band structure for the BDAVBi round rods-type PCs sample with the parameters the permittivity of the BDAVBi 3.96.

This PC has the maximum width of the complete band gap. In this case, PBG along the direction between the high symmetry points $\Gamma - M$ direction of the Brillouin Zone lies in the frequency range around $0.421(2\pi c/a)$ and $0.730(2\pi c/a)$.

When seed PCs, as shown in Figure 3, are compared with BDAVBi round rods with nematic LC infilled in Figure 5, it can be clearly seen that PBG has changed and shifted.

A comparison of Figures 4 and 5 shows that the spectra of the PCs of both types have a similar structure. This is obviously explained by the fact that these crystals have close factors of filling with dielectric materials.

The structure and material are very important for determining the optical properties of a PC structure as aforementioned. Therefore, we changed the PC structure in order to obtain optimum results. The materials' refractive index values have the same values as in the above calculations.

Table 1 shows a summary of all of these calculations. The optical properties of the 2D PC structure of BDAVBi round rods, BDAVBi round rods with air

Table 1. Optical properties of the 2D PC structure of BDAVBi round rods, BDAVBi round rods with air infilled, and BDAVBi round rods with nematic LC infilled in an air background in hexagonal lattice in TM mode.

	Band Gap				Transmission Spectrum		Equi-Frequency Surface	
	Frequency range $(2\pi c/a)$		Relative widths %				Field points per edge of unit cell	
PC in TM mode	from band 1 to band 2	from band 3 to band 4	between band 1 and 2	between band 3 and 4	Frequency range $(2\pi c/a)$		1st band	2nd band
BDAVBi round rods	0.380–0.462	0.693–0.767	19.43	10.26	0.372–0.414	0.692–0.723	6	4
BDAVBi round rods with air infilled	0.434–0.470	0.725–0.819	8.00	12.10	0.414–0.456	0.723–0.753	5	4
BDAVBi round rods with nematic LC infilled	0.395–0.464	0.703–0.797	16.19	12.51	0.384–0.426	0.700–0.730	5	4

infilled, and BDAVBi round rods with nematic LC infilled that are band gap, transmission spectrum, and equi-frequency surface are denoted in TM mode.

3.2. *Equi-frequency surface*

Because the momentum conservation law is satisfied at the reflection and refraction of waves, it is convenient to analyze the reflection and refraction of a certain wave in the space of wave numbers $\sum_{\vec{k}} = \{0; k_x, k_y, k_z\}$ by introducing the equi-frequency surface of the wave. This surface is directly described by the dispersion relation of the anisotropic medium at the fixed frequency ω. Then, the group velocity $\vec{V}_g$ of the wave in an anisotropic medium can be found as the frequency gradient in the space of wave vectors [26]. It is known that for an electromagnetic wave propagating in an anisotropic medium with a fixed frequency ω, the equi-frequency surface represents a sphere. In this case, the wave vector $\vec{k}$ and group velocity vector $\vec{V}_g$, which determines the ray direction, are always parallel. However, equi-frequency surface is not spherical for anisotropic media and the vectors $\vec{V}_g$ and $\vec{k}$ are not parallel. By analogy with the 3D case, the propagation, reflection, and refraction of the wave in a 2D structure can be described in terms of the equi-frequency dependence that can be considered as the section of the dispersion surface $\omega(k_y, k_z)$ in the space of variables $\{\omega, k_y, k_z\}$ by the plane corresponding to constant frequency. It is well known that the analysis of equi-frequency dependences is most efficient in the studies of 2D geometries, especially in solving problems when only orientations of the $\vec{V}_g$ and $\vec{k}$ vector of incident, reflected, and refracted waves are of interest, and are not the amplitudes of the reflected and refracted rays. The equi-frequency dependence has a simple physical meaning for the analysis of 2D geometries: since this dependence describes all of the possible waves with the given frequency ω and various wave vectors, the directions of the reflected and the refracted rays can be determined by simply finding the points in the equi-frequency dependences of media that satisfy the momentum conservation law at a known orientation of the boundary and a given angle of incidence of the wave.

Now, we present some numerical examples for our PC structures. In all of these examples, we exploit symmetry to calculate the equi-frequency surfaces over the irreducible Brillouin Zone of the entire Brillouin Zone.

First, we consider the equi-frequency surface of a hexagonal lattice in a dielectric medium for the $\vec{H}$ – polarization. In Figure 6, we reproduce PC with BDAVBi round rods in an air background $(\varepsilon_a = 1)$ in the hexagonal lattice parameters the lattice constant $a = 1$ μm, radius $r_1 = 0.3a$, and ordinary refractive index of BDAVBi $n_o = 1.99$. Here, the map was discretized using six field points per edge of the unit cell for the first band in Figure 6(*a*). The map was discretized using four field points per edge of the unit cell for the second band in Figure 6(*b*). The curves shown correspond to equi-frequency surfaces of the lowest order band up to frequencies just below the band gap starting at around $0.380(2\pi c/a)$.

In Figure 7, we reproduce for PC with BDAVBi round rods with air infilled in an air background for the hexagonal lattice parameters the same for BDAVBi round rods and refractive index of the air $n = 1$ for radius $r_2 = 0.15a$.

The map was discretized using five field points per edge of the unit cell for the first band in Figure 7(*a*). For the second band, the map was discretized using four field points per edge of the unit cell in Figure 7(*b*). The curves shown correspond to the equi-frequency surfaces of the lowest order band up to frequencies just below the band gap starting at around $0.434(2\pi c/a)$.

Because of the two band gaps, the band gap from bands 3 to 4 is between $0.725(2\pi c/a)$ and $0.819(2\pi c/a)$.

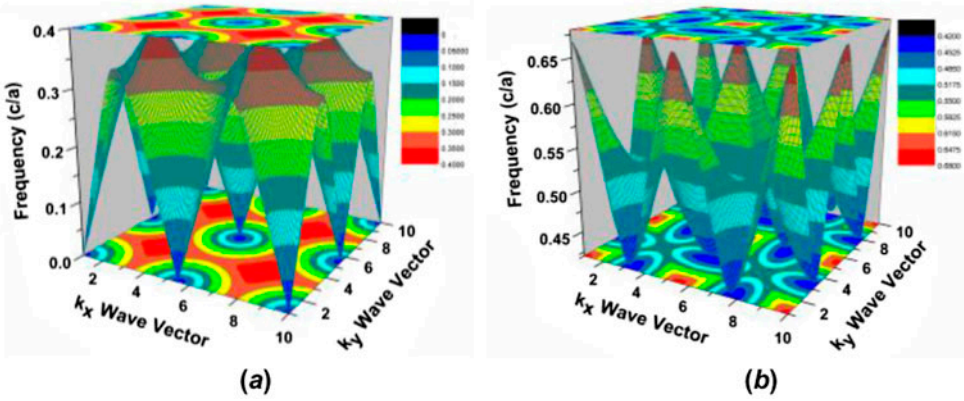

Figure 6. The equi-frequency contours of a PC with BDAVBi round rods in an air background for the hexagonal lattice (*a*) first band (*b*) second band. (The colour version of this figure is included in the online version of the journal.)

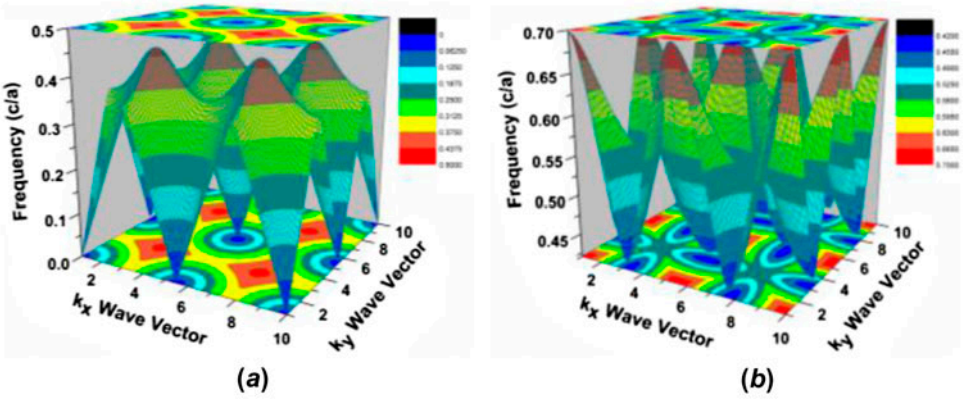

Figure 7. The equi-frequency contours of a PC with BDAVBi round rods with air infilled in an air background for the hexagonal lattice (*a*) first band (*b*) second band. (The colour version of this figure is included in the online version of the journal.)

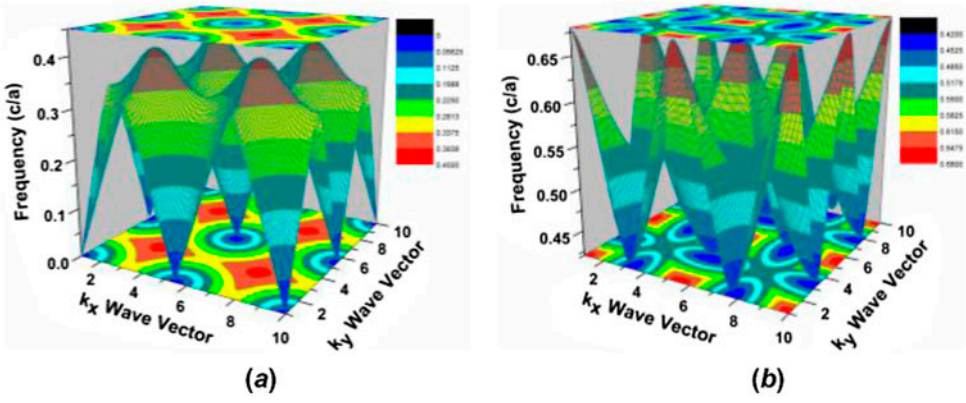

Figure 8. The equi-frequency contours of a PC with BDAVBi round rods of nematic LC infill in an air background for the hexagonal lattice (*a*) first band (*b*) second band. (The colour version of this figure is included in the online version of the journal.)

The traditional band structure plot only shows modes along the $\Gamma - M - K - \Gamma$ line. The equi-frequency contour allows us to see all of the possible wave vectors uniformly sampled in a space.

The figure uses a fixed number of sample points along each arm of the $\Gamma - M - K - \Gamma$ contour, even though the arms have different lengths. This is an important detail for estimating the shape of the contour from the band structure plot. Of course, when we calculate the equi-frequency contour, it is easy to see the shape of the contour (Figures 6–8). The circular region means isotropic propagation for the first band, while other shapes indicate anisotropic behaviors for the second band.

We reproduce for PCs, with BDAVBi round rods of nematic LC infill in an air background for the hexagonal lattice parameters, the same for BDAVBi round rods and an extraordinary refractive index of E7 type LCs $n_e = 1.7558$ for radius $r_2 = 0.15a$ in Figure 8. The map was discretized using five field points per edge of the unit cell for the first band in Figure 8(*a*). For the second band, the map was discretized using four field points per edge of the unit cell in Figure 8(*b*). The curves shown correspond to equi-frequency surfaces of the lowest order band up to frequencies just below the band gap starting at around $0.395(2\pi c/a)$.

Because of the two band gap, the band gap from band 3 to band 4 is between $0.703(2\pi c/a)$ and $0.797(2\pi c/a)$.

4. Conclusions

Computer simulation has been used to analyze the optical properties in a 2D PC structure of organic semiconductor round rods filled without and with nematic LCs in a hexagonal lattice as perspective and controlled structure for SC array. The photonic band structure for TE and TM mode is calculated along with the high symmetry point for the Brillouin zone. Furthermore, the transmittance of structure has been simulated in the visible and near IR wavelength range.

It has been shown that the dispersion of a 2D seed photonic structure in combination with the dispersion of nematic LC leads to qualitative changes in the band structure of the spectrum of the intrinsic electromagnetic excitations of the LC-infiltrated PC. This potential of reduction in reflectance, for the determined wavelengths makes it an interesting tool to improve the efficiency of any organic semiconductor-based SCs, such as standard bulk Si SCs or thin-film SCs.

In practical applications, such LC-infiltrated PCs are promising materials for use in the design of narrow band filters and a new type of optoelectronic devices.

Acknowledgments

This work is supported by the projects DPT-HAMIT, DPT-FOTON, and NATO-SET-193 and TUBA and TUBITAK under the Project Nos. 113E331, 109A015, and 109E301. One of the authors (Filiz Karaomerlioglu) would like to thank The Scientific and Technological Research Council of Turkey (TUBITAK) Postdoctoral Fellowship.

References

[1] Yablonovitch, E. *J. Opt. Soc. Am. B* **1993,** *10,* 283–295.
[2] Joannopoulos, J.D.; Johnson, S.G.; Winn, J.N.; Meade, R.D. *Photonic Crystals: Molding the Flow of Light*; Princeton University Press: Princeton, NJ, 2008.
[3] Sibilia, C.; Benson, T.M.; Marciniak, M.; Szoplik, T. *Photonic Crystals: Physics and Technology*; Springer: Italia, 2008.
[4] Sakoda, K. *Optical Properties of Photonic Crystals*; Springer: Berlin, 2005.
[5] Gupta, M.C.; Ballato, J. *The Handbook of Photonics*; CRC Press: Boca Raton, FL, 2007.
[6] Brosi, J.M. *Slow-light Photonic Crystal Devices for High-speed Optical Signal Processing*; University of Karlsruhe: Karlsruhe, 2009.
[7] Yoshino, K.; Ohmori, Y.; Fujii, A.; Ozaki, M. *Jpn. J. Appl. Phys.* **2007,** *46,* 5655–5673.
[8] Inoue, K.; Ohtaka, K. *Photonic Crystals: Physics, Fabrication and Applications*; Springer: Berlin, 2004; pp 237–260.
[9] Korkin, A.; Rosei, F. *Nanoelectronics and Photonics: From Atoms to Materials, Devices, and Architectures*; Springer: New York, 2008; pp 353–426.
[10] Noda, S.; Baba, T. *Roadmap on Photonic Crystals*; Kluwer Academic Publishers: Massachusetts, MA, 2003.
[11] Yin, Y. *Responsive Photonic Nanostructures: Smart Nanoscale Optical Materials*; RSC Publishing: Cambridge, 2013.
[12] Gaponenko, S.V.; Bogomolov, V.N.; Petrov, E.P.; Kapitonov, A.M.; Eychmueller, A.A.; Rogach, A.L.; Kalosha, I.I.; Gindele, F.; Woggon, U. *J. Luminescence* **2000,** *87–89,* 152–156.
[13] Furumi, S. *Polym. J.* **2013,** *45,* 579–593.
[14] Yokoyama, D.; Nakayama, K.I.; Otani, T.; Kido, J. *Adv. Mater.* **2012,** *24,* 6368–6373.
[15] Yokoyama, D. *J. Mater. Chem.* **2011,** *21,* 19187–19202.
[16] Taflove, A. *Advances in Computational Electrodynamics: The Finite-Difference Time-Domain Method*; Artech House: London, 1998; pp 1–30.
[17] Kittel, C. *Introduction to Solid State Physics*; John Wiley & Sons: New York, 2005.
[18] Shamery, K.A.; Rubahn, H.G.; Sitter, H. *Organic Nanostructures for Next Generation Devices*; Springer: Berlin, 2008.
[19] Myers, J.D.; Xue, J. *Polym. Rev.* **2012,** *52* (1), 1–37.
[20] Lee, K.S. *Polymers for Photonics Applications II: Nonlinear Optical, Photorefractive and Two-photon Absorption Polymers*; Springer, 2003.
[21] Hashim, A.A. *Smart Nanoparticles Technology*; InTech, Croatia, 2012; pp 561–576.
[22] Arakcheeva, E.M.; Tanklevskaya, E.M.; Nesterov, S.I.; Maksimov, M.V.; Gurevich, S.A.; Seekamp, J.; Sotomayor Torres, C.M. *Tech. Phys.* **2005,** *50,* 1043–1047.
[23] Kitamura, M.; Iwamoto, S.; Arakawa, Y. *Conference on Lasers and Electro-Optics*, Optical Society of America: CMEE3: Baltimore, MD, 2005; pp 547–549.
[24] Wu, C.; Neuner III, B.; John, J.; Milder, A.; Zollars, B.; Savoy, S.; Shvets, G. *J. Opt.* **2012,** *14,* 024005-1–024005-7.
[25] Lansey, E.; Crouse, D.T. *Proc. of SPIE* **2010,** *7772,* 777205-1–777205-12.
[26] Lock, E.H. *Physics-Uspekhi* **2008,** *51,* 375–393.